


RESEARCH ARTICLE

Open Access



# Submarine paleoseismology in the Japan Trench of northeastern Japan: turbidite stratigraphy and sedimentology using paleomagnetic and rock magnetic analyses

Toshiya Kanamatsu<sup>1\*</sup> , Ken Ikehara<sup>2</sup> and Kan-Hsi Hsiung<sup>1</sup>

## Abstract

Previous studies of sediments recovered from the Japan Trench between 37° 25' N and 38° 30' N document distinctive turbidite beds induced by huge earthquakes. We studied two sediment cores at 39°N to investigate the depositional record further north along the Japan Trench. These investigations spatially extend our knowledge of the depositional record of earthquakes in the Japan Trench. We examined specifically the precise stratigraphy of turbidite beds using paleomagnetic secular variation, and a tephra correlation. Additionally, anisotropy of magnetic susceptibility (AMS) was investigated to understand the depositional conditions of each turbidite bed. The inferred ages of turbidite beds in this study closely approximate their previously reported ages, which are correlated with the historical and prehistorical huge earthquakes off Tohoku, northeastern Japan. The paleo current directions during deposition of turbidite are inferred from their grain alignment based on AMS data. The directions of basal part reveal northeastward in the slope-side basin and north-northeast in oceanward basin. The directions of basal and upper thick muddy part of a turbidite bed are not always consistent, which suggests the hydraulic condition in the narrow elongated deep-sea basin. This fact could be essential information to elucidate a unique hydraulic condition during the turbidite deposition in the confined basin in the Japan Trench.

**Keywords** Historical earthquake, Japan Trench, Turbidite, Paleomagnetic secular variation, Paleo current, Anisotropy of magnetic susceptibility

## 1 Introduction

Intensive marine geophysical investigations have discovered structural distinctive features in the Japan Trench related to the 2011 Tohoku-oki earthquake (e.g., Kodaira

et al. 2020). Results of some studies suggest that a large displacement occurred around 38°N because of the 2011 Tohoku-oki earthquake (Fujiwara et al. 2011; Kodaira et al. 2020; Strasser et al. 2013), and this displacement led to extensive mass-wasting in the Trench. But no major bathymetric change was associated with the earthquake north of 39°N (Fujiwara et al. 2017). Fujie et al. (2020) interpreted the smectite-rich pelagic clay layer at around 39°N in the subduction sediment as having been disturbed or as having metamorphosed by an intraplate “petit-spot volcanism” (Hirano et al. 2006). They proposed that the smectite-rich pelagic clay layer around 39°N might be a barrier to the northward propagation

\*Correspondence:

Toshiya Kanamatsu  
[toshiyak@jamstec.go.jp](mailto:toshiyak@jamstec.go.jp)

<sup>1</sup> Research Institute of Marine Geodynamics, Japan Agency for Marine-Earth Science and Technology (JAMSTEC), 2-15 Natsushima-Cho, Yokosuka, Kanagawa 237-0046, Japan

<sup>2</sup> Geological Survey of Japan, National Institute of Advanced Industrial Science and Technology (AIST), Tsukuba Central 7, 1-1-1 Higashi, Tsukuba, Ibaraki 305-8567, Japan



© The Author(s) 2023, corrected publication [2023]. **Open Access** This article is licensed under a Creative Commons Attribution 4.0 International License, which permits use, sharing, adaptation, distribution and reproduction in any medium or format, as long as you give appropriate credit to the original author(s) and the source, provide a link to the Creative Commons licence, and indicate if changes were made. The images or other third party material in this article are included in the article's Creative Commons licence, unless indicated otherwise in a credit line to the material. If material is not included in the article's Creative Commons licence and your intended use is not permitted by statutory regulation or exceeds the permitted use, you will need to obtain permission directly from the copyright holder. To view a copy of this licence, visit <http://creativecommons.org/licenses/by/4.0/>.

of large, shallow coseismic slip of the 2011 Tohoku-oki earthquake.

Stratigraphy of event deposits along the Japan Trench is expected to provide spatial and temporal information related to plate boundary megathrust earthquakes as the 2011 Tohoku-oki earthquake. Evidence of historical and prehistorical huge earthquakes has often been found as onshore tsunami deposits (e.g., Sawai 2020). Furthermore, deep-sea turbidites in the Japan Trench have been reported as indication of huge earthquakes (Ikehara et al. 2016, 2017; Kioka et al. 2019; McHugh et al. 2020). The massive thick turbidite in the trench basin was attributed to the remobilization of large volumes of sediment from slopes during earthquakes. Three distinctive thick turbidite beds were discovered off Miyagi in the Japan Trench at  $\sim 38^\circ$  N (Ikehara et al. 2016). The uppermost turbidite bed is regarded as having formed during the 2011 Tohoku-oki earthquake. The next two upper turbidite beds have been correlated with the 1454 common era (CE) “Kyotoku,” and the 869 CE “Jogan” earthquakes (Ikehara et al. 2016; Bao et al. 2018). Ikehara et al. 2018 show similar turbidite beds were recognized widely in  $37^\circ 25' - 38^\circ 30' N$  along the Japan Trench. Because at least some of those turbidite beds can be regarded as the consequences of surface sediment remobilization induced by strong ground shaking (McHugh et al. 2020; Schwestermann et al. 2021), the lateral correlation of turbidite beds along the Japan Trench provides important data to elucidate not only the timing but the affected area by past huge earthquakes. This will also possibly provide some information on rupture segmentation. Based on the mentioned knowledge,  $39^\circ N$  in the Japan Trench should be a unique boundary for constraining the rupture width of not only for the 2011 Tohoku-oki earthquake but also past huge earthquakes that occurred along the Japan Trench. We, therefore, examined the distribution of turbidite along the Japan Trench as a proxy of past huge earthquake occurrences in order to explore this concept. We studied turbidite records in sediment samples taken at  $39^\circ N$  in the Japan Trench, aiming to understand whether the turbidite depositions at  $39^\circ N$  occurred simultaneously with those at the south of  $38^\circ 30' N$  previously reported, and to better understand their depositional mechanism at  $39^\circ N$ . Dating of turbidite beds is essential information for the lateral correlation of turbidite beds along the Japan Trench. Nevertheless, it is difficult to determine precise depositional ages of turbidite because of a lack of suitable methods to analyze the sediment deposited in very deep basins (over 7000-m water depth), especially for historical and prehistorical times. Kanamatsu et al. 2017, 2023 developed a dating method for turbidite

beds using paleomagnetic secular variation (PSV) records. Moreover, they found that the derived ages are well correlated with the ages of huge earthquakes from historical documents. They found that excellent PSV records are preserved in the Japan Trench sediments because of the high sedimentation rate of the hemipelagic intervals. To employ these advantages, we applied PSV stratigraphy for the lateral correlation of turbidite beds along the Japan Trench.

In contrast, the formation mechanism of turbidites with thick mud in the Japan Trench has not yet been fully understood, but their depositional mechanisms may be similar to that of “homogenite” that are related to earthquake events in a confined basin. For the homogenite, unique depositional models for explaining a thick muddy bed have been proposed based on natural observations and experiments. A suspension cloud caused by a flow rebound in a confined basin has been considered for forming the thick muddy interval (e.g., Patacci et al. 2015). The oscillating currents and seiche effects in confined basins have also been proposed by McHugh et al. (2016), Çağatay et al. (2012) and Yakupoğlu et al. (2022) for Marmara Sea, and it has been recognized in other basins such as the Canal du Sud in Haiti (e.g., McHugh et al. 2011) and most recently in the Lesser Antilles forearc basins (Morena et al. 2022). The seiche effects generated by earthquakes are considered to induce a massive structureless characteristic of “homogenite.” The seiche motion increases segregation of the fine-grained fraction and sustains the suspension (Beck et al. 2007) or induces fine-grain flows in the suspension (McHugh et al. 2016). All these studies agree in the point of oscillating currents. On the other hand, an interpretation that the thick deposits are attributed to multiple simultaneous turbidite formations induced by an earthquake (e.g., Goldfinger et al. 2012) is proposed.

We applied the anisotropy of magnetic susceptibility method (AMS) to characterize the fabric of the thick mud beds discovered in the Japan Trench. Because Campos et al. (2013) have demonstrated that AMS textural parameter is useful to distinguish homogenite, turbidite and normal hemipelagic deposits, respectively, in marine sediment in the North Central Gulf of Corinth. We also expect successful distinction between the deposits and characterization of the thick mud beds to infer their depositional mechanisms in the Japan Trench.

## 2 Methods

### 2.1 Materials

Graben and host structures have been formed as a result of the Pacific Plate subduction. These grabens and horst form basins along the strike of the Japan

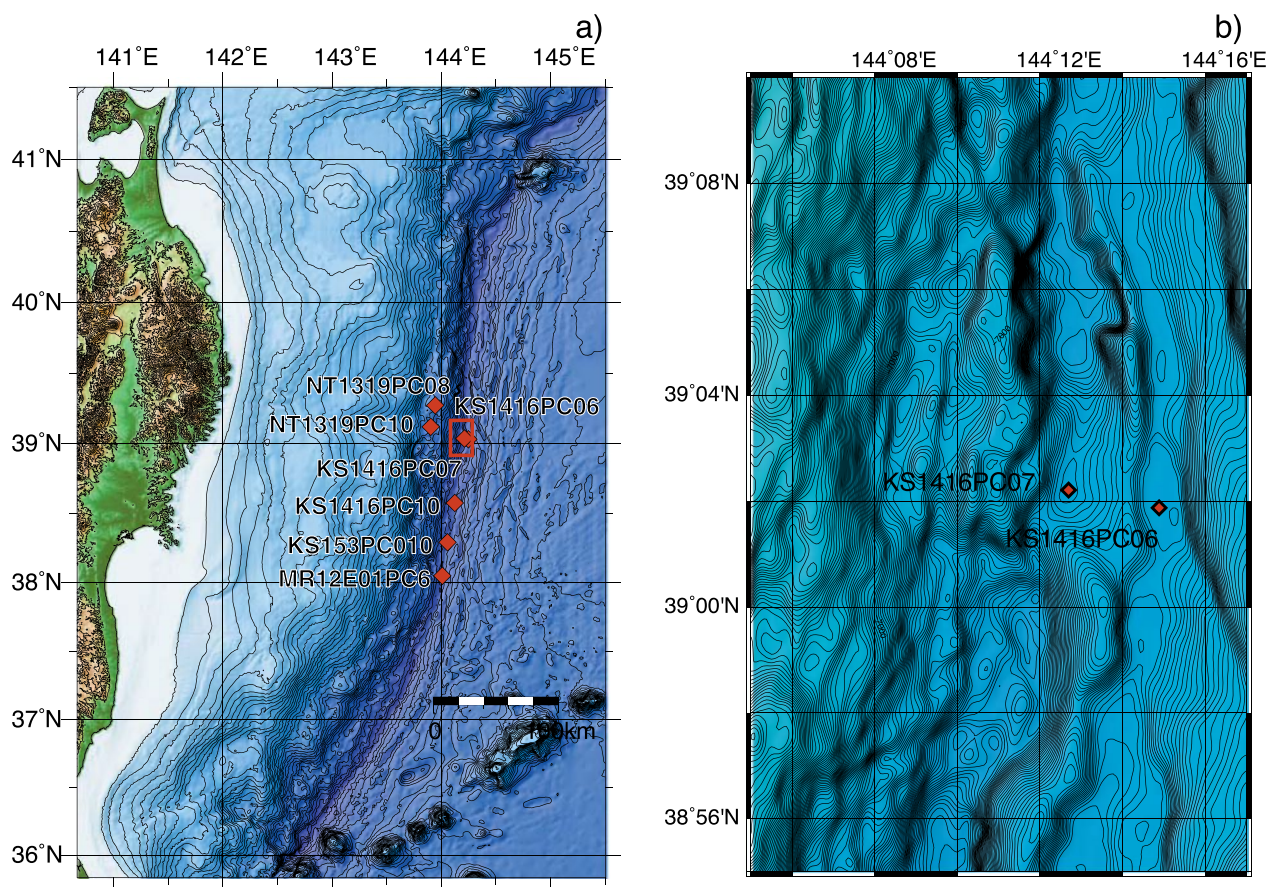


**Fig. 1** **a** Legend map of the study area: Red filled diamonds show the location of piston cores in this study and the core locations from earlier studies (Kanamatsu et al. 2017, 2023; Usami et al. 2018); the red box shows the area of **b**. **b** Detailed bathymetric map and piston core locations of cores KS1416PC06 and KS1416PC07

Trench during oblique subduction (e.g., Kobayashi et al. 1998). Sedimentary sequences infill a few to several km-width narrow basins, and this fill has been documented acoustically by Kioka et al. (2019). Piston cores KS1416PC06 (39°01.9' N, 144°14.8' E, water depth 7394 m) and KS1416 PC07 (39°02.2' N, 144°12.6' E, water depth 7282 m) were obtained in a graben basin and a trench basin, respectively. The location of core KS1416PC07 is in the trench basin near the landward slope, which is 11 km in length and less than 3 km in width. The location of core KS1416PC06 is in a graben basin east of the core KS1416PC07 that was recovered from a basin that is 30 km in length and less than 2 km in width. These basins are separated by a ridge of few hundred meters in height (horst) (Fig. 1b). The north and south extensions of KS1416PC07 basin are confined. However, the basin from where core KS1416PC06 was recovered is not confined.

The respective lithologies of cores KS1416PC06 and KS1416PC07 were reported by Ikehara et al. (2017). Their lithostratigraphy in the upper part of the

sediment cores KS1416PC06 and KS1416PC07 (Fig. 2a, h) reveals that the thick turbidite units show similarities to those reported earlier (Ikehara et al. 2016). According to the results of that study, several turbidite beds were recognized in both cores. The thicknesses of the turbidite beds range from centimeters to more than one meter. These beds are sometimes composed of a few to several amalgamated subunits. The hemipelagic intervals are recognized by the presence of bioturbation in the visual description. For this study, the turbidite beds are labeled sequentially as P6t1 to P6t9 and P7t1 to P7t6 (Fig. 2a, h). “P6” and “P7” stand for the core IDs “KS1416PC06” and “KS1416PC07.” “t” stands for turbidite, and “1” through “9” is the number of the turbidite deposit from the top to the base of the core.

Other than the turbidite and hemipelagic beds, a tephra bed containing glass shards is found in the interval between 392.2 and 394.5 cm in core KS1416PC07.

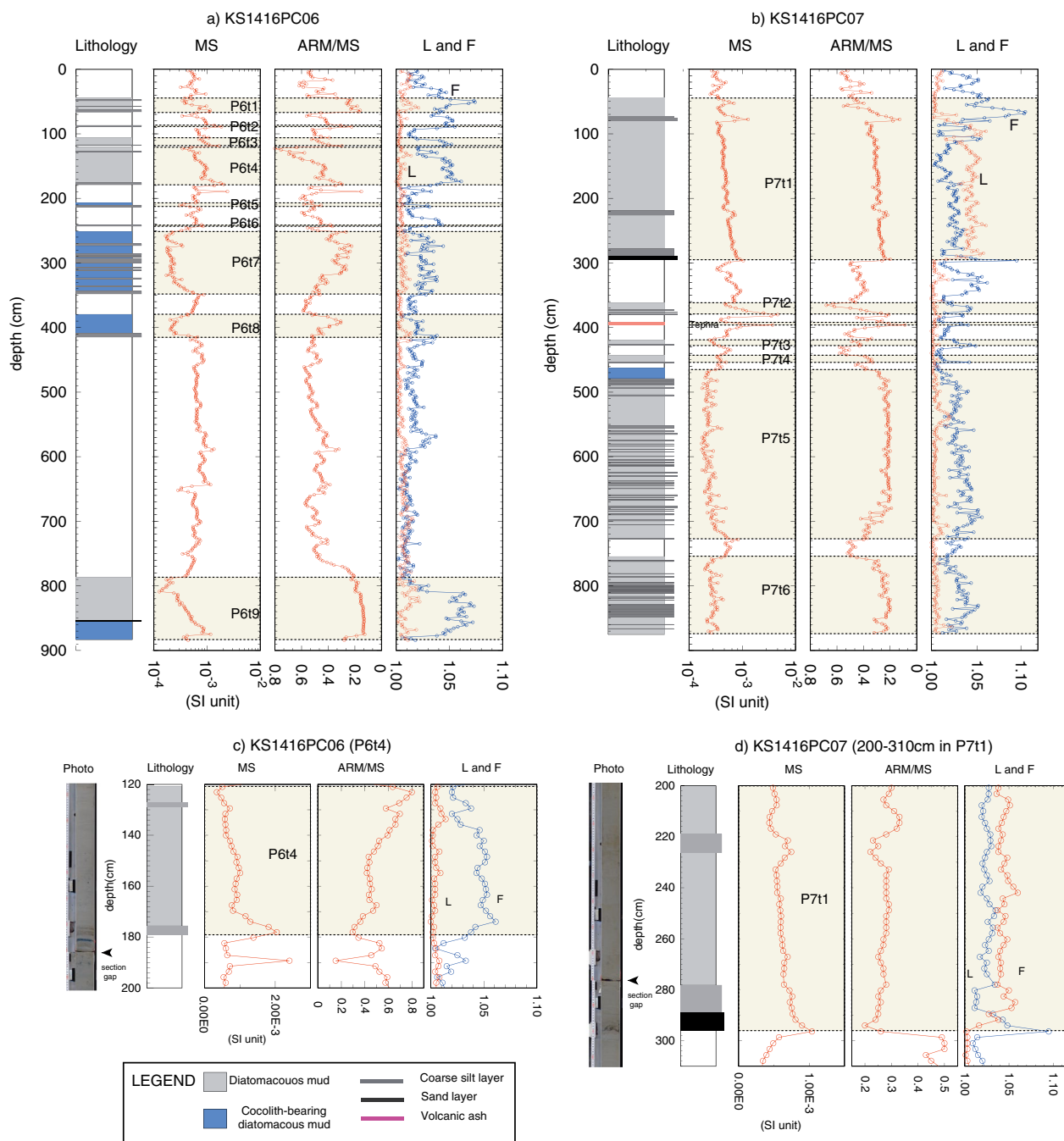


**Fig. 2** Lithology and magnetic properties of core **a** KS1416PC06; **b** KS1416PC07; **c** photo, lithology, magnetic properties of turbidite of P6t4 in KS1416PC06; **d** photo, lithology, magnetic properties of turbidite of P7t1 in KS1416PC07. MS: magnetic susceptibility; ARM/MS: ratio of Anhyseretic remanent magnetization (ARM) and MS; L: magnetic lineation (red line); F: magnetic foliation (blue line). Lithology columns are based on Ikehara et al. (2017). Legend for lithological columns: white, bioturbated diatomaceous clay-silty clay; gray, homogeneous diatomaceous clay-silty clay; blue, homogeneous nannofossil-bearing diatomaceous mud; red, volcanic ash; black thick line, sand bed; dark gray, coarse silt bed. Yellow hatches in MS, ARM/MS, L and F columns reveal the intervals of turbidite beds. The turbidite beds are labeled sequentially as P6t1 to P6t9 and P7t1 to P7t6. "P6" and "P7" stand for the core IDs "KS1416PC06" and "KS1416PC07." "t" stands for turbidite, and "1" through "9" is the number of the turbidite deposit from the top to the base of the core

## 2.2 Sample analysis

Paleomagnetic and rock magnetic samples (2.2-cm square plastic cube) were taken from halved sections of cores KS1416PC06 and KS1416PC07. The remanent magnetizations were measured using a superconducting rock magnetometer (2G Enterprises model 760) at Japan Agency for Marine-Earth Science and Technology (JAMSTEC). All the samples were demagnetized with alternating field demagnetization (AFD) at stepwise levels of 5mT between 0 and 40 mT, and 10 mT between 50 and 80 mT. Natural remanent magnetization (NRM) was measured after each demagnetization treatment. Anhysteretic remanent magnetization (ARM) was imparted in an 80 mT alternating field with a 0.1 mT direct field. The inclinations, declinations and maximum angular deviation (MAD) values of NRM of all the sample were calculated using software (PuffinPlot; Lurcock and Wilson 2012).

Aiming at documenting the thick-turbidite textural characteristics using magnetic properties, the magnetic susceptibility (MS) and its anisotropy (AMS) were measured using KLY-4 (Agico Inc.) at JAMSTEC. Directions and magnitudes of three principal susceptibility axes: maximum ( $K_{max}$ ), intermediate ( $K_{int}$ ) and minimum ( $K_{min}$ ), are obtained by these measurements. The AMS parameters “L” ( $K_{max}/K_{int}$ ) for characterizing the linearity and “F” ( $K_{int}/K_{min}$ ) for characterizing the oblateness of samples are calculated from magnitudes of three principal susceptibilities to determine the shape of the magnetic fabric (Tarling and Hrouda 1993). Other rock magnetic measurements were performed to investigate the sample’s magnetic properties. The measurements of the hysteresis loop (max applied field 1 T) were carried out by a vibrating sample magnetometer (VSM, model 2900; Princeton Measurements Corp.) on the selected samples from the hemipelagic interval. Saturation remanent magnetization ( $M_r$ ), saturation magnetization ( $M_s$ ) and coercive force ( $H_c$ ) were obtained after removing paramagnetic contributions. We also ascertained the coercivity of the remanence ( $H_{cr}$ ) of each sample by applying progressively increasing backfields after saturation at 1 T.

Also, isothermal remanent magnetization (IRM) acquisition experiments were performed on those samples with 4 mT step up to 1 T by VSM. After being saturated by 1 T, the backfield of 0.3 T was imparted. The S-ratio proposed by Bloemendal et al. (1992) was calculated for the samples to estimate magnetic mineralogy. We consider that the magnetic particle size is very informative to recognize turbidite depositional structures such as fining upward. It was investigated using the simple proxy of ferrimagnetic grain size (ARM/MS) (Banerjee et al. 1981; King et al. 1982), which changes inversely with magnetic particle size that is increasing in the range of 1–10  $\mu\text{m}$  (e.g., Stoner et al. 1996).

**Table 1** Tie point between cores and ARCHE3k.1 data

	ARCHE3k.1 Age (year)	PC06 depth* (cm)	PC07 depth* (cm)
<i>Declination point</i>			
B	923 CE	78.0	119.3
C	105 BCE		169.9
D	939 BCE		
<i>Inclination point</i>			
a	1672 CE		25.2
b	1225 CE		61.8
c-	475 CE	86.8	142.3
d	238 CE	110.0	

\*Depth after turbidite removing

The obtained paleomagnetic data were compared to a master curve of secular variation (ARCH3k.1: Korte et al. 2009), which was generated through compilation between 0 and 3 ka archeomagnetic data. ARCH3k.1 has been also used in previous studies of the Japan Trench (Kanamatsu et al. 2017, 2023), because the master curve is suitable for paleomagnetic field studies in Europe and Asia, and reliable for the Northern hemisphere data (Donadini et al. 2009). We used “StratFit” software (Sagnotti and Caricchi 2018) to compare the obtained paleomagnetic data to the master data. The tie points were selected as apparent peaks and troughs in the inclination and declination profiles (Table 1). Using “StratFit,” we obtained the age of each core.

One tephra bed was identified in the interval between 392.2 and 394.5 cm in core KS1416PC07. The morphology and refractive index of the volcanic glass shards and the mineral composition of the bed were assessed by Kyoto Fission Track Ltd., Kyoto, Japan, for correlation with earlier reported tephra deposits in the Japan Trench.

Radiocarbon age using bulk organic carbon (OC  $^{14}\text{C}$ ) was conducted for two hemipelagic samples from core KS1416PC06 and two hemipelagic samples from KS1416PC07 to compare the result of PSV results. The radiocarbon age determinations were conducted at Beta Analytics Co., Ltd., USA. Acid (HCl) was applied to ensure the absence of carbonates in the samples as preparation of radiocarbon age determination at Beta Analytics Co. Ltd.

## 3 Results

### 3.1 Depth variation of magnetic parameters

The profiles of magnetic susceptibility (MS), ARM/MS (parameters for magnetic grain size), AMS parameters “L” and “F” with depth are plotted in Fig. 2. Sharp peaks of MS are generally found in silt to very fine

sand beds corresponding to bases of turbidite beds in intervals between 0 and 200 cm (P6t1–P6t6) in core KS1416PC06, and between 0 and 400 cm (P7t1–P7t5) in core KS1416PC07 (Fig. 2b, g). In P7t1, multiple fining-upward intervals are observed (ARM/MS in Fig. 2b). MS shows an increase at the base of turbidite (288 cm). It decreases gradually toward the top of the deposit. Prominent MS peaks occur at 58 cm and 80 cm within P7t1. MS decreases upward up to 45 cm and 60 cm, respectively, in their signals.

Among all the turbidite beds, the highest peaks of MS occur at 198 cm in P6t4 and at 380 cm in P7t2, respectively.

In addition to MS peaks of turbidites, the tephra bed also shows a prominent MS peak similar to those of the coarser component of the turbidites, which are in the tephra bed at 398 cm in core KS1416PC07.

Analysis by ARM/MS reveals an approximate mirror image with MS above 180 cm in core KS1416PC06 (Fig. 2a) and above 400 cm in KS1416PC07 (Fig. 2b). The ARM/MS indicates a larger grain size at the base of turbidite beds. For example, a coarser grain size at the base of P7t2 than that of the underlying hemipelagic interval and a gradual decrease upward are observed. Those features are interpreted as arising from the fining-upward of the turbidite beds.

However, below 180 cm (P6t5–P6t9) in core KS1416PC06, and 400 cm (P7t3–P7t6) in core KS1416PC07, a sharp peak of MS does not always occur in the turbidite bases. Also, ARM/MS show no upward decreasing pattern. Moreover, MS of P6t5–P6t9 and P7t3–P7t6 is markedly weaker than those of overlying and underlying hemipelagic intervals. Referring to MS data of hemipelagic intervals in the studied cores (Fig. 2a, b) and the other trench sites (Fig. 8a–c); however, MS values reveal rather constant ranges between  $10^{-3}$  and  $10^{-4}$  order. It is interpreted that MS of hemipelagite is not affected significantly by diagenesis in the Japan Trench. Then, it is interpreted that the weak MS of P6t5–P6t9 and P7t3–P7t6 reflects the primal component and content of turbidite or is due to pyritization and subsequent MS decrease within the turbidite (e.g., Johnson et al. 2021).

The ARM/MS in turbidite is considered to reflect grain size change during turbidite deposition, which could make difference from the magnetic grain size of bioturbated hemipelagite.

### 3.2 Magnetic fabric

Results of AMS measurements are used to investigate the sediment fabric of the turbidite beds to better understand the depositional mechanisms. Because of the

small number of data (less than three) in the very thin to thin beds, we excluded P6t2, P6t5 and P6t7 from the evaluation.

Actually “L” is generally low: close to 1.0 in both cores of KS1416PC06 and KS1416PC07 (Fig. 2d, h), except for the interval between 60 and 300 cm in core KS1416PC07.

Some turbidite beds reveal increasing “F” around their bases (P6t3, P6t8, P7t1, P7t3, P7t4, P7t5). High “F” value does not occur always at the base of turbidite bed. For example, P6t4 shows high “F” values at upper depth from the turbidite base (Fig. 2c).

AMS directions are orientated by the mean of paleomagnetic declination of the cores. The AMS directions (Kmax, Kint and Kmin) of the turbidite beds are plotted on the lower hemisphere equal-area projections (Fig. 3a). Along with the turbidite beds, the AMS of all the hemipelagic intervals in each core is shown, respectively, in Fig. 3b.

Three patterns of AMS directions are recognized based on the directional distributions of Kmax and Kmin.

1. A girdle formed by Kmax axes (e.g., P6t9 in Fig. 3a, P7t5 in Fig. 3a). The girdle plane of this type is slightly oblique to the horizontal plane. The Kmin axes slightly deviate from the vertical axes.
2. Kmax axis distribution shows strong clustering, and Kmin axes form a girdle around the Kmax axis (e.g., P7t1 in Fig. 3a).
3. Kmax axes are scattered in the horizontal plane of equal-area projection (e.g., KS1416PC07 in Fig. 3b). Kmin is well clustered, perpendicular to the horizontal plane.

### 3.3 Remanent magnetization

Simple decrease in horizontal and vertical magnetic components during AFD experiments reveals stable single component in most samples (Fig. 4a, b). Saturations of IRM around 300 mT and the S-ratio ranging about 0.98 in the selected samples indicate that the magnetization is carried by low coercive force magnetic minerals, such as magnetite. Ratios  $M_{rs}/M_s$  and  $H_{cr}/H_c$  of the hysteresis parameter plotted in Day diagram (Day et al. 1977) indicate that the values range in the pseudo-single domain state (Fig. 4c).

Figure 5a–c shows plots of the component-analyzed inclination and declination. The declination is expressed as a relative declination with  $\Delta D_{95}$  and  $\Delta I_{95}$  (95% confidence level converted from MAD; Khokhlov and Hulot 2016). The  $\Delta D_{95}$  and  $\Delta I_{95}$  are mostly large at the turbidite intervals, indicating that the obtained magnetic directions are unstable. A large break exists in the declination

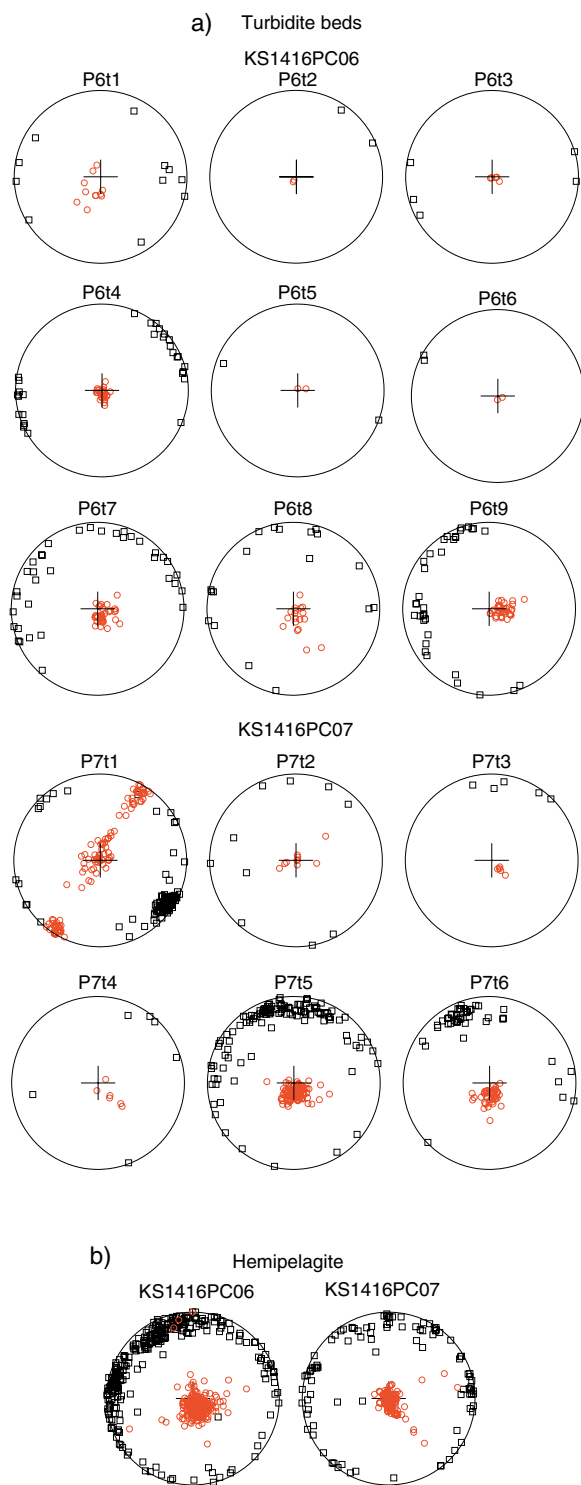


**Fig. 3** AMS principal magnetic susceptibility directions projected on the lower hemisphere in an equal-area projection: Kmax (black open box) and Kmin (red open circle) of **a** turbidite beds in cores KS1416PC06 and KS1416PC07, and **b** AMS directions of hemipelagite intervals in cores KS1416PC06 and KS1416PC07

variation at 65 cm and the scattered in the interval above 65 cm in core KS1416PC06 (Fig. 5a), which might have been horizontally twisted during piston coring or during handling or the core sample operations before taking the subsamples. The values of  $\Delta D_{95}$  and  $\Delta I_{95}$  are also high in 0–65 cm in core KS1416PC06 (Fig. 5a, b), indicating that some artificial influence might have affected the magnetization. In accordance with the observations above, the interval was excluded from the paleomagnetic interpretation.

### 3.4 Tephra

The tephra bed at 392.2–394.5 cm in KS1416PC07 (Fig. 2b) is 2.3 cm thick, coarse silt in grain size, and consisting of fibrous pumice-type glass fragments, which is a glass type of “T” in the definition by Yoshikawa et al. (1976). Green-colored hornblende is a dominant heavy mineral. Opaque minerals and orthopyroxene are present as minor components. The refractive indices of the volcanic glass shards range from 1.5047 to 1.5091 (mode: 1.507). These petrographic features are consistent with the Haruna-Futatsudake-Ikaho (Hr-FP) tephra which was previously reported on land, and in marine sediments off Sanriku (Tables 2, and 3 in Ikehara et al. 2018), the occurrence of the Hr-FP tephra in marine sediments is restricted strongly to around 39–40°N (Fig. 3B in Ikehara et al. 2018). This distribution is also consistent with the location of KS1416PC07, in which Hr-FP tephra is found. The erupted age of Hr-FP tephra is considered to have in the sixth century (Soda 1989). Geshi and Oishi (2011) show a conventional median age of  $^{14}\text{C}$  as 1480 yr BP for eruption age of Hr-FP, and it was considered as a year range of cal. 555–615 CE (68.2% probability). Okuno et al. (2019) obtained a year range of cal. 424–444 CE, and interpreted that the age of Hr-FP eruption is estimated to be cal. 538–559 CE (79.0% probability) taking the local offsets of  $^{14}\text{C}$  of trees into consideration.

## 4 Discussion

### 4.1 PSV record

Because NRM of turbidite is largely subjected by grain alignment of turbidite deposition (e. g. Tanty et al. 2016), NRM direction of turbidite beds does not reflect geomagnetic field directions. Therefore, NRM of turbidite beds must be excluded from the paleomagnetic stratigraphic interpretation (Kanamatsu et al. 2017, 2023). Both the coarse base and the fine intervals of turbidites were removed and left with only the hemipelagic intervals. The boundary between turbidite and hemipelagite can be recognized from rock magnetic parameters of MS and ARM/MS (see Sect. 3.1).

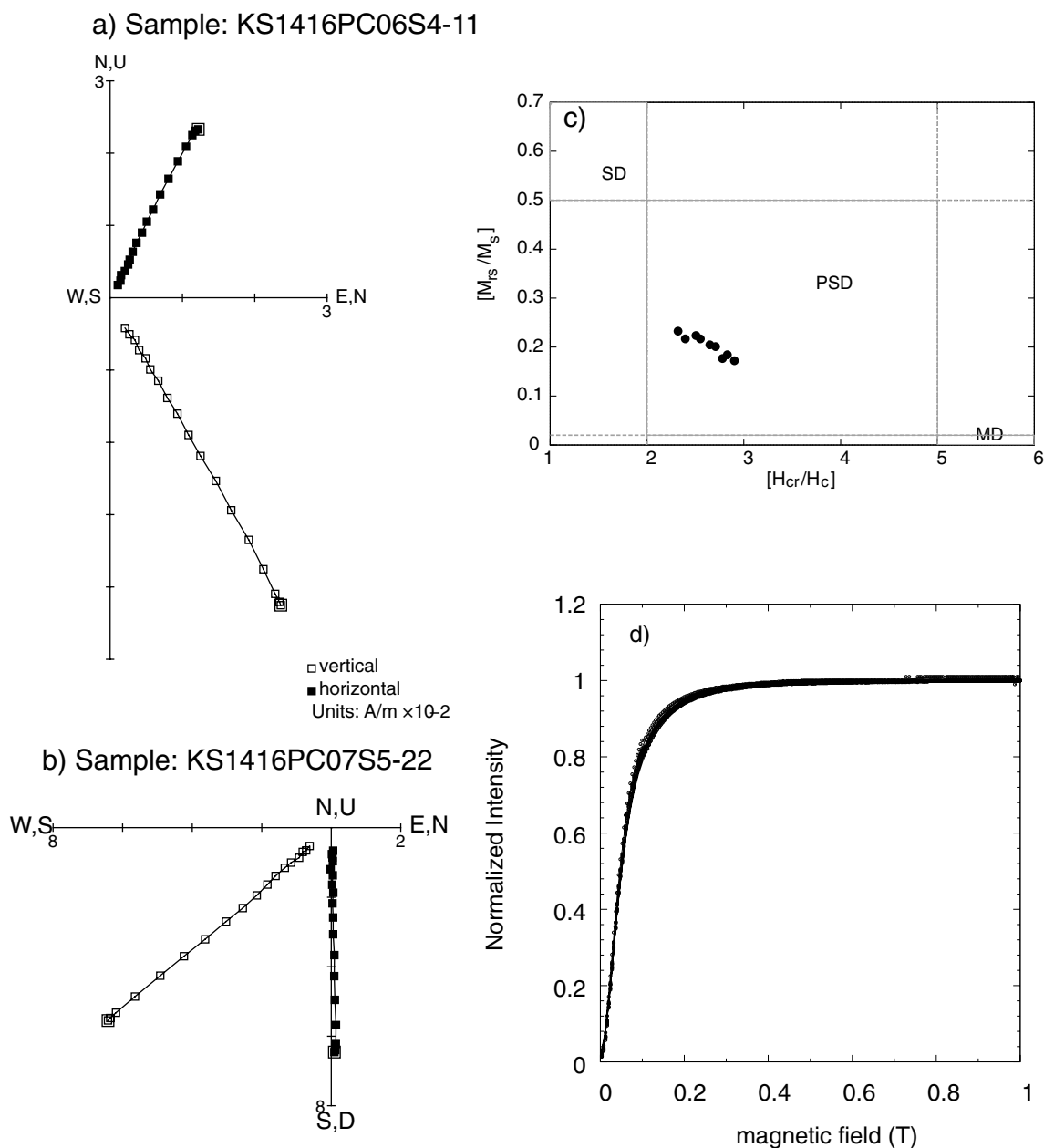


**Fig. 4** Orthogonal projections of AFD experiment. **a** Sample KS1416PC06S4-11 and **b** sample KS1416PC07S5-22: **c** “Day plot” (Day et al. 1977) for hemipelagic samples. SD, PSD and MD, respectively, denote single domain, pseudo-single domain and multidomain fields. **d** Stepwise IRM acquisition experiments on 9 samples ()

PSV data constructed by removing turbidite intervals are used to estimate the depositional age of the turbidite beds (Fig. 6a). After removing the turbidite data, we recalculated the depth of the paleomagnetic data assuming no large gaps in deposition (Fig. 5). In fact, P6t3 and P6t4 are different turbidite beds which are separated by 2 cm hemipelagite. But because thickness is smaller than resolution of sampling (2.2 cm), we

regard that the both beds deposition occurred at the same time.

The obtained paleomagnetic data of core KS1416PC07 are correlated with ARCH3k.1 with a tephra key bed (Fig. 6b). Under the assumption that the sedimentation rates of the hemipelagic intervals in KS1416PC07 are similar to that of core KS1416PC06, we compare the paleomagnetic data using “StratFit” (Fig. 6b). The



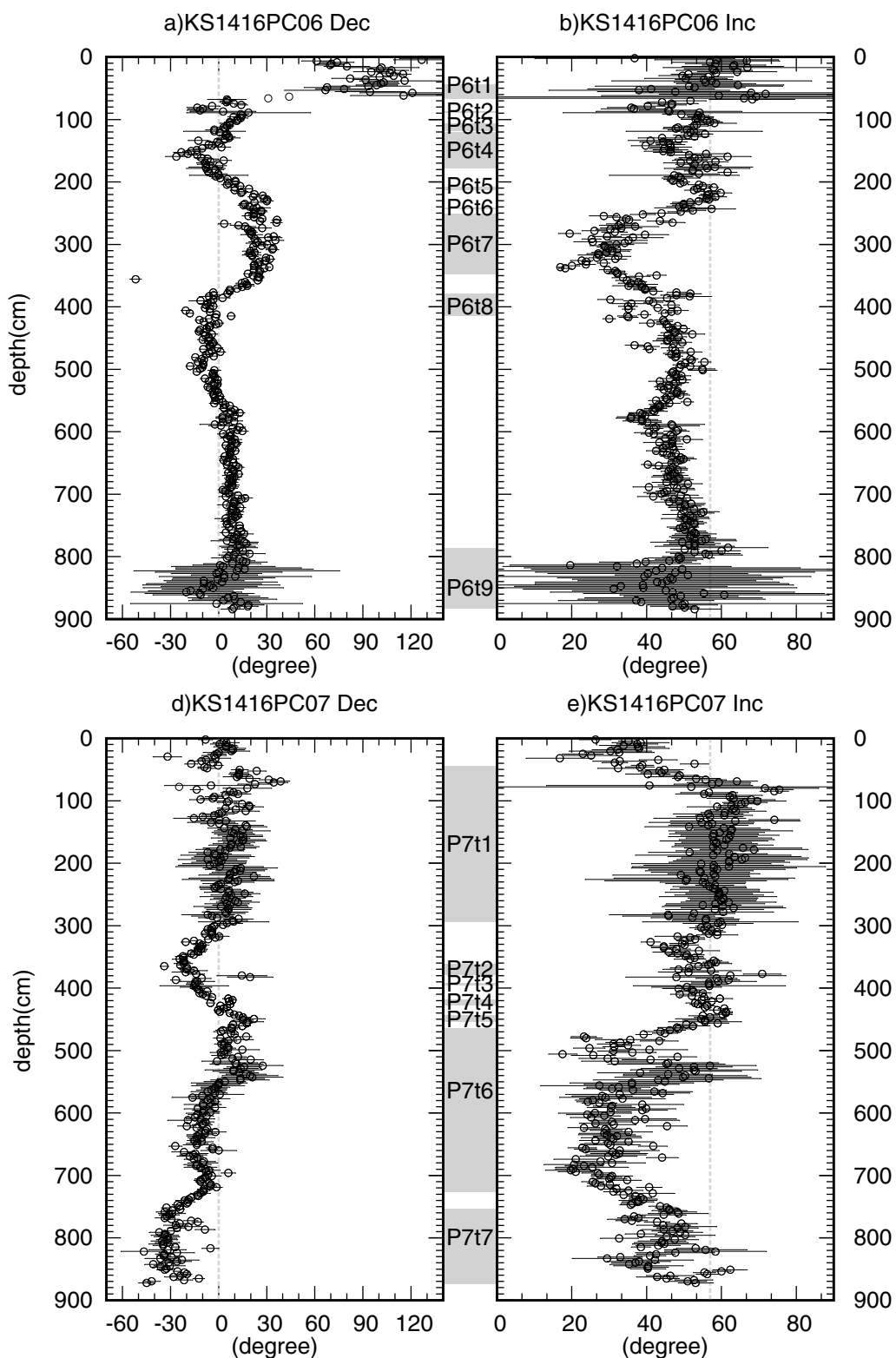


**Fig. 5** **a, e** declination data with 0° (gray broken line) for cores KS1416PC06 and KS1416PC07, and **b, d** inclination data with GAD inclination (gray broken line) for cores KS1416PC06 and KS1416PC07, respectively.  $\Delta D_{95}$  and  $\Delta I_{95}$  (Khokhlov and Hulot 2016) shown with declinations and inclinations. Gray hatched intervals indicate turbidite beds

**Table 2** Ages of turbidite units based on PSV correlation

Turbidite bed no.	CE (year)
P6t1	–
P6t2	–
P6t3	978 ( $\pm$ 127)
P6t4	978 ( $\pm$ 127)
P6t5	343 ( $\pm$ 127)
P6t6	– 45 ( $\pm$ 127)
P6t7	– 301 ( $\pm$ 127)
P6t8	– 720 ( $\pm$ 127)
P6t9	< – 5948
P7t1	1254 ( $\pm$ 131)
P7t2	833 ( $\pm$ 131)
P7t3	233 ( $\pm$ 131)
P7t4	– 8 ( $\pm$ 131)
P7t5	– 171 ( $\pm$ 131)
P7t6	< – 635

paleomagnetic tie points (Table 1; Fig. 6b) and the eruption age of Hr-FP found in core KS1416PC07 are used. The sedimentation rates of the hemipelagic intervals in KS1416PC07 are 81.4 cm/kyr, and that of KS1416PC06 is 71.2 cm/kyr. Because the reference curve is only available for data up to 3000 years ago, for the older periods, the age is obtained from the extrapolation using the sedimentation rate of that of above interval. (The results are available in Additional file 1)

The calculated ages of the turbidites are shown in Table 2. Turbidites that can be correlated between cores

KS1416PC06 and KS1416PC07 based on age are shown with broken lines in Fig. 6.

#### 4.2 Accuracy and uncertainty of PSV dating

Validity of assignment of PSV correlation has been inspected using OC  $^{14}\text{C}$  (Table 3). Although it has been reported that OC  $^{14}\text{C}$  in hemipelagite is significantly older than those of depositional age in the Japan Trench due to the mixing of old organic matter, the linear relationship between age and depth suggests a possible deposition age with consideration of an age offset (Ikehara et al. 2016; Bao et al. 2018; Kioka et al. 2019; Schwestermann et al. 2021; Usami et al. 2021). We estimated the offset of OC  $^{14}\text{C}$  using a hemipelagite sample at 13 cm below the Hr-FP (sample KS1416 PC07 sec6-15 in Table 3), which is to be 170 years older than the Hr-FP horizon based on its sedimentation rate. We regard 1480 BP as a Hr-FP eruption age which is reported in Geshi and Oishi (2011). The OC  $^{14}\text{C}$  age of hemipelagite samples is considered as ca 2,200 years older in the study area. The corrected OC  $^{14}\text{C}$  ages, taking into account the 2,200 years offset (Table 3), and the ages obtained from the PSV (Table 2) are plotted together in Fig. 7. The plots show a general agreement between the estimated OC  $^{14}\text{C}$  and PVS ages and support the validity of PSV correlation of cores KS1416PC06 and KS1416PC07, although the nature of OC  $^{14}\text{C}$  makes it difficult to justify the accuracy of the PSV.

Considering the discrete data interval of 2.2 cm for this study, time intervals corresponding to one discrete sample of KS1416PC06 and KS1416PC07 are 31 yrs. and 27 yrs., respectively, based on the sedimentation rate

**Table 3** Results of radiocarbon age determinations

Sample name	Depth (cm)	Depth after turbidite removing (cm)	Conventional age (BP year)	*Corrected age (BP year)
KS1416PC06 s2-12	23.4–25.5	23.4–25.5	2090 $\pm$ 30	– 110 $\pm$ 30
KS1416 PC06 s4-18	221.8–223.9	110.5–112.7	4160 $\pm$ 30	1940 $\pm$ 30
KS1416 PC07 s5-20	43.6–45.9	75.6–77.9	3480 $\pm$ 30	1260 $\pm$ 30
KS1416 PC07 s6-15	407.6–409.9	125.5–127.8	3870 $\pm$ 30	1650 $\pm$ 30

\*Corrected age, taking into account the 2200 years offset

(See figure on next page.)

**Fig. 6** Declination and inclination data after removal of turbidite intervals: **a** declination of KS1416PC06, **b** declination of KS1416PC07, **c** declination of Archeo3k.1. **d** inclination of KS1416PC06, **e** inclination of KS1416PC07, **f** inclination of Archeo3k.1, respectively.  $\Delta D_{95}$  and  $\Delta I_{95}$  are also shown for declinations and inclinations. Broken lines indicate the horizon of turbidite beds. A–D, a–e are tie points used in correlation between core data and Archeo3k.1. **g** Fitting KS1416PC06 declination data (red line) to that of Archeo3k.1 (gray line), **h** KS1416PC06 inclination data (red line) to that of Archeo3k.1 (gray line), **i** KS1416PC07 declination data (red line) to that of Archeo3k.1 (gray line), **j** KS1416PC07 inclination data (red line) to that of Archeo3k.1 (gray line)

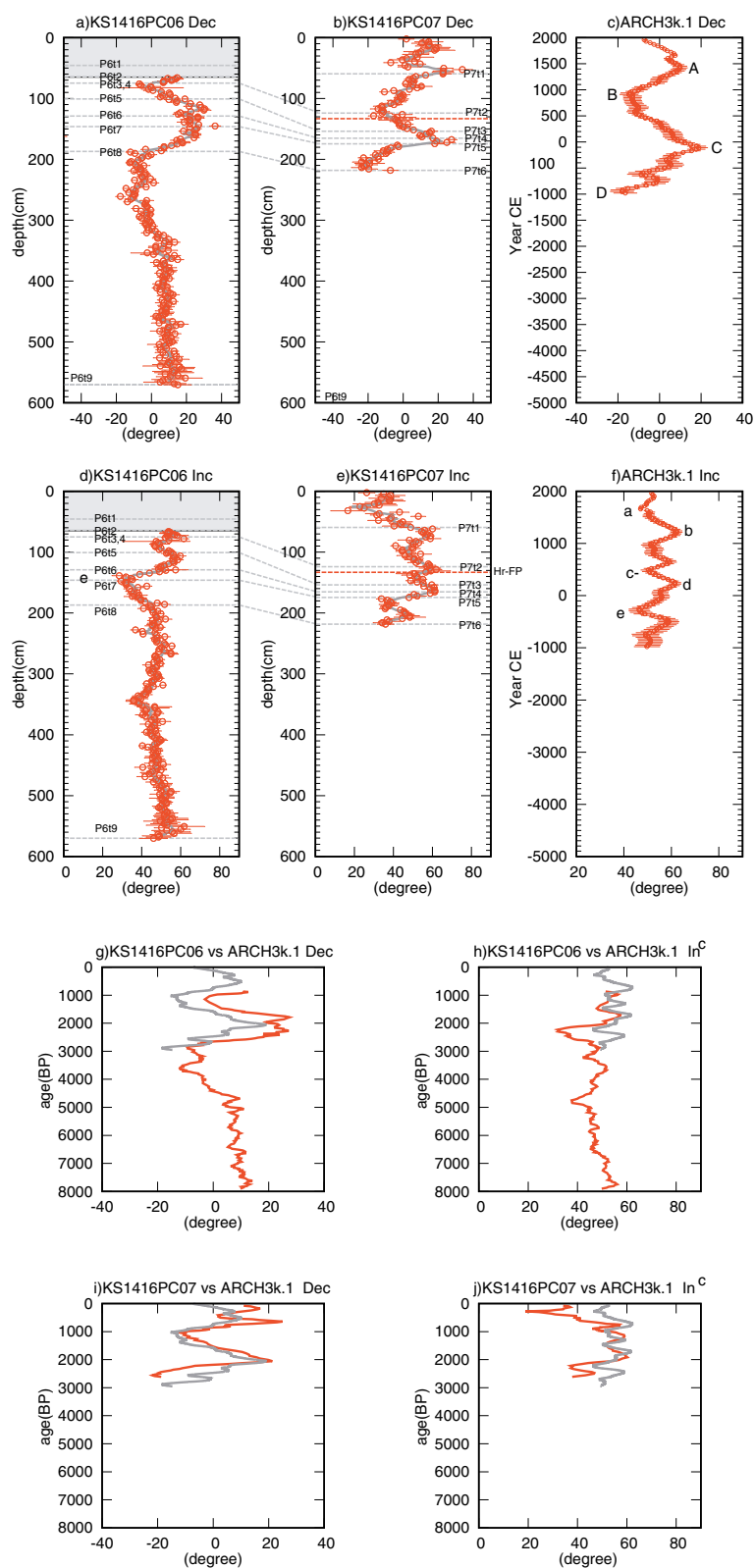


**Fig. 6** (See legend on previous page.)

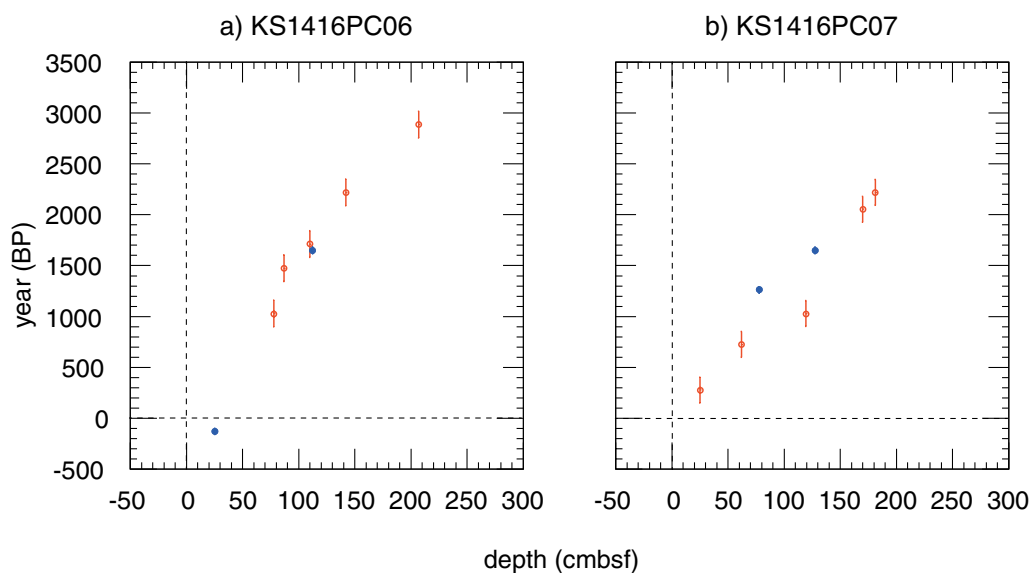


**Fig. 7** Ages of offset bulk  $^{14}\text{C}$  dates (blue; Table 3) versus ages derived from PSV (red; Table 2) correlation of cores KS1416PC06 and KS1416PC07. Lines in vertical axes (year) show error bars

of KS1416PC07 (81.4 cm/kyr) and that of KS1416PC06 (71.2 cm/kyr). Taking maximum uncertainty of ARCH3k data (100 years; Donadini et al. 2009) into account, the uncertainties for one data point would be within ranges of 131 and 127 years for KS1416PC06 and KS1416PC07. The obtained ages should include those uncertainties.

#### 4.3 Correlation using PSV dating

The stratigraphy of turbidite beds from the previous studies and this study is summarized by comparing records of synchronous turbidite beds in Fig. 8. Ages of  $978 \pm 127$  CE of P6t3 and P6t4 and  $833 \pm 131$  CE of P7t2 agree to 869 CE “Jogan earthquake” within the uncertain ranges, and also close to the turbidite ages previously reported (Table 2), which are 972 CE (14t3 of core KS1416PC10 in Fig. 8c) and 881 CE (15t3 of core KS1503PC10 in Fig. 8b).

Age of  $1254 \pm 131$  CE of P7t1 is close to the 1454 CE “Kyotoku earthquake.” Although it is out of the range of uncertainty, P7t1 should be correlated with “Kyotoku earthquake” because of no other large earthquake around this time in the historical record. P6t7 ( $301 \pm 127$  BCE) and P7t5 ( $171 \pm 131$  BCE) are close to the ages of turbidite BCE 283 (14t4 of core KS1416PC10 in Fig. 8c) and BCE 128 (15t5 of core KS1503PC10 in Fig. 8b), which are regarded having been deposited at 2.3 ka. The other comparable pair of turbidites is P6t8 ( $720 \pm 127$  BCE) and P7t6 ( $635 \pm 131$  BCE) judged from their ages.

In the previous studies (Ikehara et al. 2016; Bao et al. 2018, Kanamatsu et al. 2022), turbidite beds formed by the 2011 Tohoku-oki earthquake are well documented in the trench between  $38^\circ\text{N}$  and  $38^\circ30'\text{N}$  (Fig. 8a–c). In

this study (in the trench at  $39^\circ\text{N}$ ), we cannot conclude the existence of 2011 turbidite in the cores by paleomagnetic and rock magnetic analyses. However, the slope sediments at  $39^\circ\text{N}$  (in NT1319 PC10 and PC08 located 30 and 35 km east, respectively, from KS1416PC07) have evidences of the 2011 Tohoku-oki earthquake (e.g., McHugh et al. 2016; Usami et al. 2018). In fact, McHugh et al. (2016) measured excess  $^{210}\text{Pb}$  in steady state in the upper 16 cm of both cores. Surface sediment remobilization is related to this large enrichment of excess  $^{210}\text{Pb}$ , so that it is a possible interpretation that the 2011 turbidites were formed in the trench basins, but failed to be sampled during coring. Another possibility is sensitivity of turbidity-current generation to the earthquake ground shaking. Usami et al. (2018) indicate that the slope sediments have records of great ( $M_w \sim 8$ ) and giant ( $M_w \sim 9$ ) earthquakes clearly above Hr-FP in the slope sediment cores; however, the record of great ( $M_w \sim 8$ ) earthquakes is not obvious in the trench (KS1416PC07) at  $39^\circ\text{N}$ . This observation suggests the sensitivity of turbidity-current generation to earthquake ground shaking is different locally.

We also cannot clearly define the turbidite corresponding to Kyotoku earthquake (1454 CE) in core KS1416PC06 because of disturbed paleomagnetic record, while the turbidite recognized in KS1416PC07 is 260-cm thick and its magnetic fabric in the lower and middle intervals is interpreted to be formed under a strong current because their rolling  $K_{\text{max}}$  axes are considered to be formed perpendicular to a strong flow. The ARM/MS reveals finning upward overall in P7t1. The Kyotoku

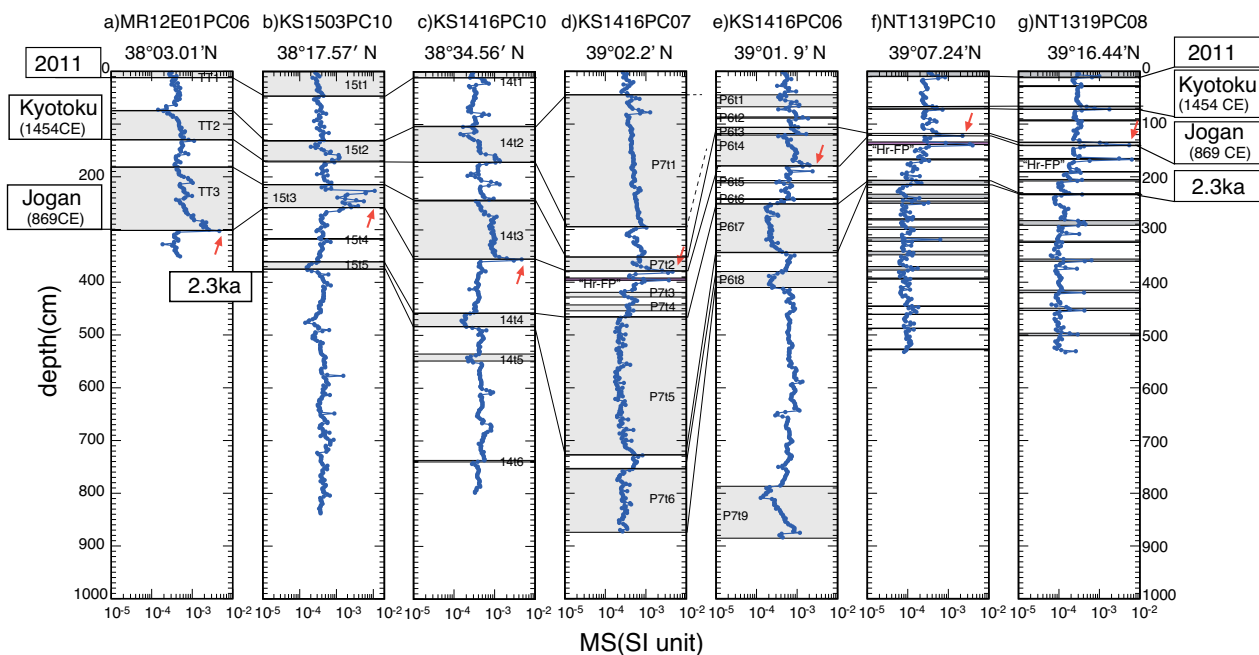


**Fig. 8** Contemporaneous turbidite beds and magnetic susceptibility profiles in the Japan trench basins and the slope basins: cores KS1416PC10 and KS153PC10 (Kanamatsu et al. 2023); cores NT1319PC10 and NT1319PC8 (redrawn from Kanamatsu et al. 2017). Red arrows indicate high magnetic susceptibility peaks. Black line shows turbidites correlation in the studied cores. Note scales of horizontal axes (MS) are expressed by log scale

turbidites in the southern area are several tens cm in thickness, and their AMR/MS variations are also characterized by fining upward. The Kyotoku turbidites are also recognized in cores NT1318PC08 and NT1318PC10 (Usami et al. 2018), although the layer thickness is thinner (Fig. 8f, g).

The thickness of Jogan turbidite (869 CE) is 18 cm in KS1416PC07, and 60 cm in KS1416PC06. In the southern area, thickness of the beds is several tens cm (Fig. 8). Their ARM/MS variations of Jogan turbidites show clear fining upward except KS1503PC10. High magnetic susceptibility values are observed in the bases of Jogan turbidites in the all the sites (Fig. 8). The occurrence of a “Jogan (869 CE)” turbidite (P7t2) just above the 6th-century Hr-FP tephra layer is stratigraphically consistent (Fig. 8d). Jogan turbidites are also recognized in cores NT1318PC08 and NT1318PC10 with thinner thicknesses. Thus, “Jogan” turbidites are distributed both on the landward slope and on the trench axis around 39°N.

“2.3 ka” turbidites reported in the previous study (Kanamatsu et al. 2023) can be correlated with P6t7 and P7t5 in this study, and to the T5 beds in cores NT1318PC10 and NT1318PC08 (Usami et al. 2018) by PSV correlation (Kanamatsu et al. 2023).

Thickness of “2.3 ka” turbidites in the south area is a few tens cm. 260 cm and 90 cm are in KS1416PC07 and KS1416PC06, respectively. Magnetic susceptibility

of “2.3 ka” turbidites in the trench basins is remarkably weaker than those of overlying and underlying hemipelagic intervals.

Because the thicknesses of the turbidite reflects flow hydrodynamics, initial sediment volume and depositional local setting such as topography, interpretation of their variation is difficult. However, the occurrence of “Kyotoku,” “Jogan” and “2.3 ka” turbidites is confirmed based on the paleomagnetic chronology in the trench basins. These occurrences suggest that the turbidite depositions observed in the southern area occurred simultaneously in also 39°N area. The occurrence of turbidite beds formed in 1454 CE (Kyotoku), 869 CE (Jogan), 2.3 ka and probably 2011 CE extends to 39°N from the south, indirectly corresponding rupture zone of those large earthquakes.

The uppermost part of core KS1416PC07 is thought to have been deposited at about 1900 CE based on the PSV data (Fig. 8). The interval of KS1416PC07 between “Kyotoku” (1454 CE) and 1900 CE involves no distinct thick turbidite bed as it was for the older thick turbidites, whereas within that time interval, the records of tsunami and tsunami deposits along the coast off Tohoku are well documented of the 1611 CE Keicho and 1896 CE Meiji Sanriku tsunamis (e.g., Sawai et al. 2020). Turbidites corresponding to 1896 CE Meiji Sanriku are also found in the slope sediments off the central Tohoku (Usami et al. 2018) and the northern Tohoku (Ikehara et al. submitted).

Although no indication as turbidite, small magnetic susceptibility peaks and fining upward patterns in ARM/MS observed in core KS1416PC07 may be an event deposit related to the Meiji Sanriku earthquakes judged from its stratigraphic position (Fig. 2).

#### 4.4 Magnetic fabric

AMS directions are used to presume local current flow direction during turbidite bed depositions. Axes of the magnetic susceptibility are reorientated by the mean directions of paleomagnetic declination of the cores. Because the paleomagnetic data of P6t1 are not available, AMS direction of P6t1 is without directional reconstruction.

Under a hydraulic flow, Kmax axes could be parallel to a flow direction, whereas perpendicular Kmax to the current direction is formed in a strong flow, which roll grains over the surface (e.g., Tarling and Hrouda 1993; Baas et al. 2007).

Taira and Scholle (1979) proposed an AMS fabric evolution in a turbidite deposition. They demonstrated the relationship between the shape type and orientation of principle AMS axes, and turbidite depositional environments, which is defined by divisions of the Bouma sequence (Bouma 1962). They demonstrated in the basal part of turbidite that “subdivision A” is characterized by perpendicular Kmax distribution to the flow direction and tilting Kmin upstream (imbrication). They revealed that Kmax orientation in the upper part of “division A,” and “divisions B and C,” changes to be parallel to the flow direction. The imbrication angle dipping to upstream is gradually shallow. Consequently, the Kmax direction can be parallel and perpendicular to a flow direction during turbidite deposition. It implies that the flow analysis using only Kmax direction is difficult without understanding the depositional environment of the “subdivision” of turbidite. For this study, we, therefore, use the Kmin dipping direction to investigate a local current direction as suggested by Tarling and Hroud (1993).

Shallower of Kmin inclinations is observed around the base of turbidite beds (Figs. 9 and 10), and in several cm from the base of turbidite beds, for example, in P6t4 (Fig. 9) and P7t5 (Fig. 10), respectively. This observation indicating an imbricated fabric around the basal interval is consistent with the magnetic fabric evolution model presented by Taira and Scholle (1979).

We divided AMS directions of a turbidite bed into a basal sandy interval and an upper muddy interval, because depositional conditions of the two intervals could be different in confined basins as described in “Introduction.”

The divided AMS directions of turbidite beds are shown in Figs. 9 and 10. We regard mean Kmin

dipping directions as current directions for turbidite beds (Table 4).

A dominant AMS direction in the basal sandy intervals for core KS1416PC07 (Fig. 10) is revealed to south-east, whereas the dominant AMS direction for core KS1416PC06 (Fig. 9) is to south-southeast. (P6t1 is an exception due to no paleomagnetic data.) By contrast, the directions of the upper muddy intervals are diverse. Some sites show no prevailing flow direction of muddy portion indicated by vertical Kmin (e.g., P6t4, P7t1u1 in Figs. 9 and 10). It is interpreted as a deposition under still hydraulic conditions. Polonia et al. (2017) documented “a clayey silt cap” in the homogenite as being deposited as part of the tsunamite due to its chemical composition. McHugh et al. (2016) interpreted the sediments enriched in  $^{134}\text{Cs}$  and  $^{137}\text{Cs}$  radioisotopes derived from the Fukushima nuclear reactors found on top of the mid-slope terrace cores as settling through the water column post-Fukushima and post-tsunami. These interpretations could be applied to explain no preference direction fabric in, e.g., P6t4 and P7t1u1.

In the most cases of muddy upper intervals, the AMS directions are slightly oblique to their basal directions (e.g., P6t7, P6t8 in Fig. 9, P7t3, P7t4 in Fig. 10). The smaller changes in flow directions are suggested during the upper interval depositions. In the thick upper portion of P7t5 (Fig. 10), the intervals are subdivided into several beds based on directions. They are changing frequently, but the major direction seems to be southward.

AMS directions of upper intervals in two beds (P6t1 in Fig. 8 and P7t2 in Fig. 10) show anti-parallel directions to their basal directions, although AMS of P6t1 bed is not reorientated by paleomagnetic directions. AMS of P7t2 indicates that an eastward flow in the initial depositional stage changed to a westward flow in the upper muddy deposition. Those changes may be occurred by deflection and reflection of currents which were controlled by topographical constrains (e.g., Patacci et al. 2015). The oblique flow directions observed in many cases could be explained by deflection of flows from the initial flow, which is oblique to north–south extending edges of basins (Fig. 1b). The reversed direction of P7t2 could be explained by a reflection of eastward flow against the west facing ridge of the basin.

The general consistent directions among basal beds of each core may implicate an initial mechanism controlling the direction during initial deposition. Their local slope topography may be a possible control factor which constrain the flow pathway. The steep slope west side to core KS1416PC07 location could have induced southeastward flows (Fig. 1b). In contrast, the south-southeast directions in core KS1416PC06 suggest flows along the basin axis (Fig. 1b). The cause of the different directions of flow

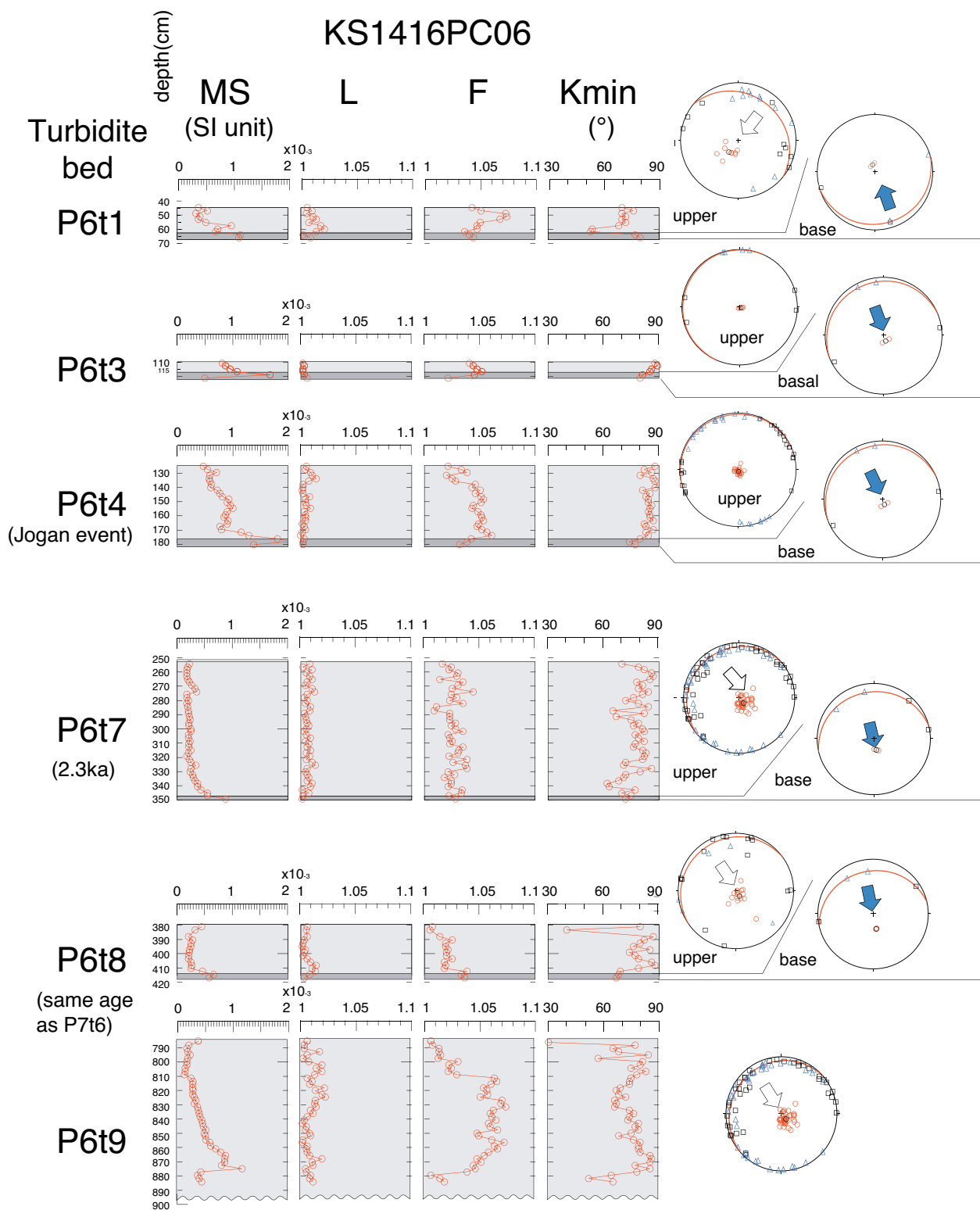


**Fig. 9** AMS data of core KS1416PC06. Magnetic susceptibility (MS), “L” and “F” and Kmin inclinations of each turbidite beds and stereo plots of with inferred pale flow. Blue filled arrows, basal sandy interval; white arrow, upper muddy interval; orange arrows, possible shearing, shorting, or rolling directions. Great circle perpendicular to the Kmin is drawn in red lines

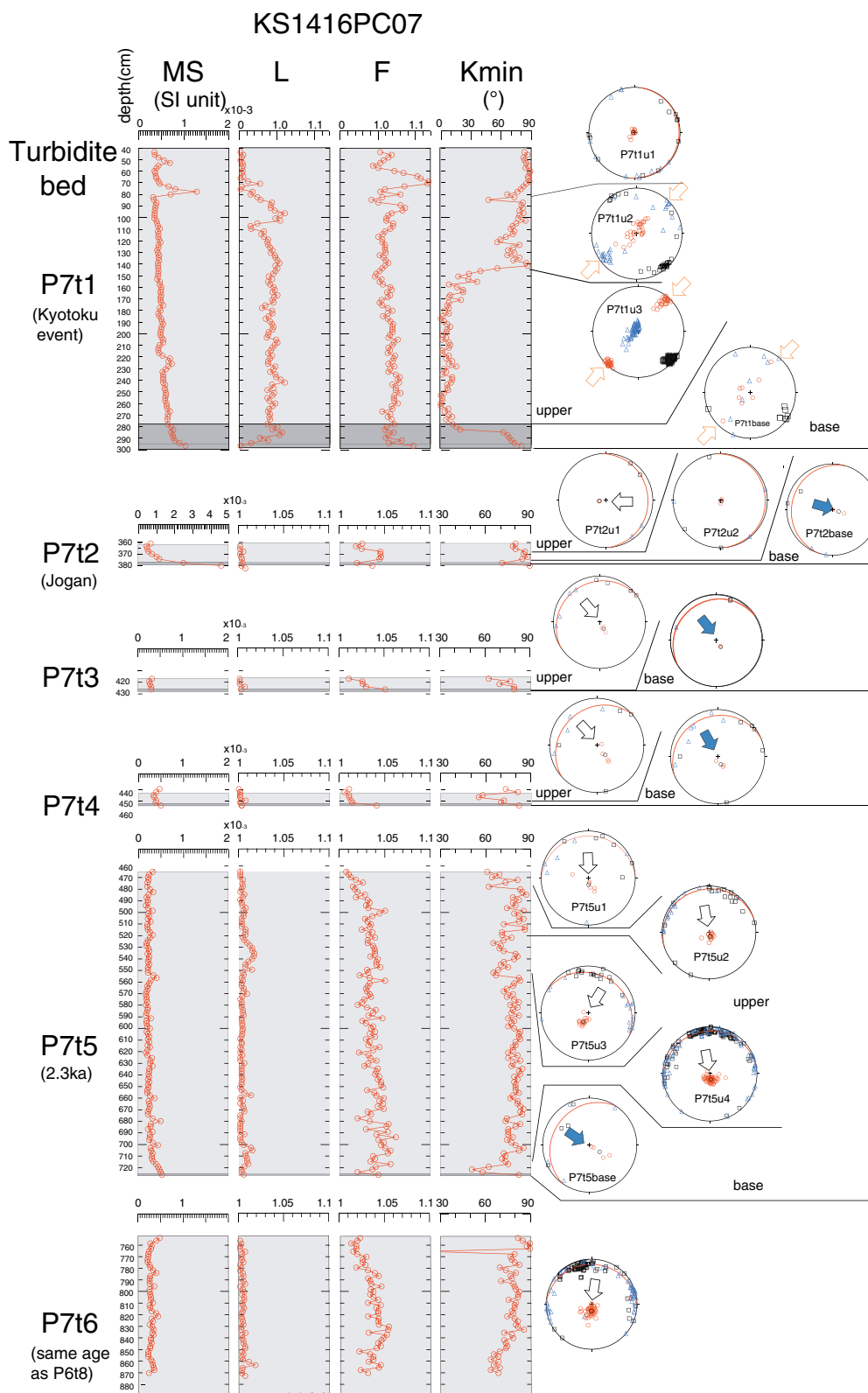


**Fig. 10** AMS data of core KS1416PC07. Magnetic susceptibility (MS), "L" and "F" and Kmin inclinations of each turbidite beds and stereo plots of with inferred pale flow. Blue filled arrows, basal sandy interval; white arrow, upper muddy interval; orange arrows, possible shearing, shorting, or rolling directions. Great circle perpendicular to the Kmin is drawn in red lines



**Table 4** Mean Kmin direction (vertical axis to magnetic foliation) of turbidite beds and hemipelagic intervals of cores KS1416PC06 and KS1416PC07

Bed no. (subbed)	Sample no.	Declination	Inclination	$\alpha_{95}$	Kappa
P6t3	4	114	88	3.6	645.2
P6t3 base	2	157.6	82.1	23.7	113.5
P6t4	25	161.7	87.3	1.9	229.8
P6t4 base	2	168.6	75.5	6.6	724.6
P6t7	39	136	80	3	59.1
P6t7 base	2	166.7	73.7	13.4	174.5
P6t8	15	145.4	81.3	7.2	27.5
P6t8 base	2	167.5	67.5	3.3	2833.5
P6t9	44	97.6	77.7	4.4	25.3
P7t2u1	2	265.8	79	4.7	143.3
P7t2u1	3	107	88.2	6.4	250.6
P7t2 base	2	107.4	78.5	47.5	14.9
P7t3	4	147.1	76.3	5.6	200.9
P7t3base	1	146	78	–	–
P7t4	4	138	67.7	17.4	21.7
P7t4 base	2	164.9	76.9	34.4	27.4
P7t5u1	6	177.2	78.5	14.8	21.5
P7t5u2	14	162	82.8	3.5	131.5
P7t5u3	17	209.6	73.4	3.4	112.4
P7t5u4	69	170.5	80.4	1.6	109
P7t5base	4	124.3	69.4	20.4	21.3
P7t6	51	181.3	77.5	3.5	34.3
P7 hemipelagite	79	129.9	84.7	3.1	28.2
P6 hemipelagite	245	151.5	79.9	1.6	32.6

k Fisherian precision parameter,  $\alpha_{95}$  radius of cone of 95% confidence

in the muddy upper interval may not only occur from basin properties (accommodation space, morphology, axis direction, etc.) but flow thickness, flow density and initial flow direction of turbidity flows.

The AMS variation of P7t1 is greatly in contrast to the other AMS axis directional patterns (Fig. 10). P7t1 is subdivided into three intervals based on AMS directions. The AMS direction of the basal part (P7t1base) can be interpreted as rolling of the Kmax directions perpendicular to a strong flow, suggesting northeastward or southwestward. However, the Kint axes become well clustered in vertical and the Kmin axes horizontal in P7t1u3 with the horizontal Kmax direction. The Kint and Kmin directions of the P7t1u2 are regard as similar to that of P7t1base. P7t1base and P7t1u2 can be interpreted as having been formed under strong flows from the northeast or southwest. Also, P7t1u1 has Kmax and Kint scattered in a horizontal plane: a direction under still hydraulic condition. However, horizontal Kmin and vertical Kint

of P7t1u3 are enigmatic directions as sedimentary fabric. This type is usually reported as “prolate type” indicating layer parallel shearing or layer parallel shortening (e.g., Pares 2015), although we have no evidence based on data from this study to discuss the possibility of deformation.

#### 4.5 Magnetic fabric of hemipelagite

The AMS directions in all the hemipelagic intervals of core KS1416PC07 (Fig. 3b) show no preferred orientation in Kmax, suggesting a still hydraulic condition during deposition. By contrast, the AMS direction of hemipelagite in core KS1416PC06 is indicated as southward (Fig. 3b). The obtained direction of KS1416PC06 may suggest the exist of bottom current during hemipelagite deposition. The basin of core KS1416PC06 is not confined, but that the basin of core KS1416PC07 is an enclosed basin (Fig. 1b). This topographical setting would allow a flow entering from north in the basin of core KS1416PC06, but restrict a flow entering in the basin of core KS1416PC07 site, if a deep current system exists in the trench floor. Although no study of deep-sea bottom current on the floor of Japan Trench over 7000 m has been reported, several reports have described long-term steady bottom currents in both landward (southward flow) and seaward (northward flow) slopes along the Japan Trench as deep western boundary currents in ~6000 m water depth (Mitsuzawa et al. 1998, Fujio and Yanagimoto 2005). Mitsuzawa et al. (1998) reported the deep western boundary current flows south-southwest in the landward slope of the Japan Trench with mean speed of 3–7 cm/s and maximum speed of 15–20 cm/s. On the other side, a deep bottom current in the abyssal plain in the east of Japan Trench reveals westward (Owens and Warren 2001, Fujio and Yanagimoto 2005). AMS study for surface sediments in the abyssal plain east of the Japan Trench (Kawamura et al. 2015) revealed the AMS directions as generally parallel to the deep bottom current in the abyssal plain. Because a flow of more than 1 cm/s current can form imbricated magnetic fabric (Taring and Hrouda 1993), a few cm/s of bottom current might generate the flow pattern in AMS in the hemipelagite.

AMS data of turbidite basal sandy beds indicate a flow to southeast at core KS1416PC07 location, and south-southeast at core KS1416PC06 location. However, the directions of most thick muddy intervals of turbidite beds are not always consistent with those of their basal sandy intervals. These AMS directions indicate no consistent flow direction during thick muddy part of turbidite and suggest a complex hydraulic condition in the elongated small basin. Although more dense spatial AMS data should be necessary to confirm the flow evolution in the confined basin, we demonstrated the possibility that the

AMS method might be able to reconstruct the complex flow pattern.

## 5 Conclusion

1. Turbidites of ages in two cores corresponding to the 1454 CE “Kyotoku,” 869 CE “Jogan” and “2.3 ka” were recognized in the Japan Trench floor at 39°N as confirming finding from earlier reported piston core samples obtained at 38°–38°30′N.
2. High magnetic susceptibility was widely observed for the turbidites corresponding to the Jogan earthquake. The “Jogan” turbidite at 39°N is associated with a distinct MS peak arising from tephra “Hr-FP” just below the turbidite horizon. These clear signatures will be useful for identification of the “Jogan” turbidite around 39°N.
3. Paleo-flow directions of turbidites based on the magnetic fabric in each core show that the directions from the basal sandy interval and the upper muddy interval in one turbidite bed are not always consistent. The prevailing directions in the basal intervals of turbidites are recognized in each location as south-eastward at core KS1416PC07 location in the landward trench basin, while to south-southeastward at core KS1416PC06 site in the graben basin.

### Abbreviations

PSV	Paleosecular variation
CE	Common era
NRM	Natural remanent magnetization
ARM	Anhyseretic remanent magnetization
AMS	Anisotropy of the magnetic susceptibility
MAD	Maximum angular deviation
Hr-FP	Haruna-Futatsudake-Ikaho tephra

### Supplementary Information

The online version contains supplementary material available at <https://doi.org/10.1186/s40645-023-00545-3>.

**Additional file 1. Table S1:** Declination, inclination, and age data of KS1416PC06 which are used for calculation of turbidite ages. Inc: inclination, dec: declination. **Table S2:** Declination, inclination, and age data of KS1416PC07 which are used for calculation of turbidite ages. Inc: inclination, dec: declination.

### Acknowledgements

We thank the captains, officers, crew, and scientific party of the KS-14-16 cruise. K. Tsuchida provided excellent technical support throughout this study. We also thank Drs. K. Usami and R. Hino for their useful suggestions. We thank Dr. Cecilia M. McHugh and an anonymous reviewer for their helpful comments, which have improved the manuscript.

### Author contributions

TK led conducted magnetic measurements, constructed the age model and drafted the manuscript. KI conducted the sedimentological analyses and tephra analysis. KH conducted interpretation of magnetic results. All authors have read and approved the final manuscript.

### Funding

This work was supported by Japan Society for the Promotion of Science (KAKENHI) Grant No. 19H05596 (Representative: Hino R).

### Availability of data and materials

Obtained data in this study are presented in tables and supplemental data. For other data, please contact the corresponding author to request data.

### Declarations

#### Competing interests

The authors declare that they have no competing interest.

Received: 29 August 2022 Accepted: 12 March 2023

Published online: 28 March 2023

### References

- Baas JH, Hailwood EA, McCaffrey WD, Kay M, Jones R (2007) Directional petrological characterisation of deep-marine sandstones using grain fabric and permeability anisotropy: methodologies, theory, application and suggestions for integration. *Earth Sci Rev* 82:101–142. <https://doi.org/10.1016/j.earscirev.2007.02.003>
- Banerjee SK, King J, Marvin J (1981) A rapid method for magnetic granulometry with applications to environmental studies. *Geophys Res Lett* 8:333–336. <https://doi.org/10.1029/GL008i004p00333>
- Bao R, Strasser M, McNichol AP, Haghypour N, McIntyre C, Wefer G, Eglinton TI (2018) Tectonically triggered sediment and carbon export to the Hadal zone. *Nat Commun* 9:121. <https://doi.org/10.1038/s41467-017-02504-1>
- Beck C, Mercier de Lépinay B, Schneider JL, Cremer M, Çağatay MN, Wendenbaum E, Boutareaud S, Menot G, Schmidt S, Weber O, others (2007) Late Quaternary co-seismic sedimentation in the Sea of Marmara's deep basins. *Sediment Geol* 199(1–2):65–89. <https://doi.org/10.1016/j.sedgeo.2005.12.031>
- Bloemendal J, King JW, Hall FR, Doh SJ (1992) Rock magnetism of late Neogene and Pleistocene deep-sea sediments: relationship to sediment source, diagenetic processes, and sediment lithology. *J Geophys Res* 97:4361–4375
- Bouma AH (1962) *Sedimentology of some flysch deposits*. Elsevier, Amsterdam
- Çağatay MN, Erel L, Bellucci LG, Polonia A, Gasperini L, Eris KK, Sancar Ü, Biltekin D, Uçarkus G, Ülgen UB, Damci E (2012) Sedimentary earthquake records in the Izmit Gulf, Sea of Marmara, Turkey. *Sed Geol* 282:347–359. <https://doi.org/10.1016/j.sedgeo.2012.10.001>
- Campos C, Beck C, Crouzet C, Demory F, Van Welden A, Eris K (2013) Deciphering hemipelagites from homogenites through anisotropy of magnetic susceptibility. Paleoseismic implications (Sea of Marmara and Gulf of Corinth). *Sediment Geol* 292:1–14. <https://doi.org/10.1016/j.sedgeo.2013.03.015>
- Day R, Fuller MV, Schmidt A (1977) Hysteresis properties of titanomagnetites: grain-size and compositional dependence. *Phys Earth Planet Inter* 13:260–267. [https://doi.org/10.1016/0031-9201\(77\)90108-X](https://doi.org/10.1016/0031-9201(77)90108-X)
- Donadini F, Korte M, Constable CG (2009) Geomagnetic field for 0–3 ka: 1. New data sets for global modeling. *Geochem Geophys Geosys* 10:Q06007. <https://doi.org/10.1029/2008GC002295>
- Fujie G, Kodaira S, Nakamura Y, Morgan J, Dannowski A, Thorwart M, Greve-meyer I, Miura S (2020) Spatial variations of incoming sediments at the northeastern Japan arc and their implications for megathrust earthquakes. *Geology* 48(6):614–619. <https://doi.org/10.1130/G46757.1>
- Fujio S, Yanagimoto D (2005) Deep current measurements at 38°N east of Japan. *J Geophys Res* 110(C2). <https://doi.org/10.1029/2004JC002288>

- Fujiwara T, Kodaira S, No T, Kaiho Y, Takahashi N, Kaneda Y (2011) The 2011 Tohoku-oki earthquake: displacement reaching the trench axis. *Science* 334(6060):1240. <https://doi.org/10.1126/science.1211554>
- Fujiwara T, dos Santos FC, Bachmann AK, Strasser M, Wefer G, Sun T, Kanamatsu T, Kodaira S (2017) Seafloor displacement after the 2011 Tohoku-oki earthquake in the northern Japan Trench examined by repeated bathymetric surveys. *Geophys Res Lett* 44:11833–11839. <https://doi.org/10.1002/2017GL075839>
- Geshi N, Oishi M (2011) The 14C ages of the late Pleistocene-Holocene volcanic products erupted from the Haruna volcano. *Bull Geol Surv Jpn* 62(3/4):177–184 (in Japanese with English abstract)
- Goldfinger C, Hans Nelson C, Morey AE, Johnson JE, Patton JR, Karabanov E, Gutierrez-Pator J, Eriksson AT, Gracia E, Dunhill G, Enkin RJ, Dallimore A, Vallier T (2012) Turbidite event history: methods and implications for Holocene paleoseismicity of the Cascadia subduction zone. In: USGS Professional Paper, 1661-F, p 184. US Geological Survey. <https://doi.org/10.3133/pp1661f>
- Hirano N, Takahashi E, Yamamoto J, Abe N, Ingle SP, Kaneoka I, Kimura J, Hirata T, Ishii T, Ogawa Y, Machida S, Suyehiro K (2006) Volcanism in response to plate flexure. *Science* 313:1426–1428. <https://doi.org/10.1126/science.1128235>
- Ikehara K, Kanamatsu T, Nagahashi Y, Strasser M, Fink H, Usami K, Irino T, Wefer G (2016) Documenting large earthquakes similar to the 2011 Tohoku-oki earthquake from sediments deposited in the Japan Trench over the past 1500 years. *Earth Planet Sci Lett* 445:48–56
- Ikehara K, Usami K, Kanamatsu T, Danhara T, Yamashita T (2017) Three important Holocene tephras off the Pacific coast of the Tohoku region, Northeast Japan: implications for correlating onshore and offshore event deposits. *Quatern Int* 456:138–153. <https://doi.org/10.1016/j.quaint.2017.08.022>
- Ikehara K, Usami K, Kanamatsu T, Arai K, Yamaguchi A, Fukuchi R (2018) Spatial variability in sediment lithology and sedimentary processes along the Japan Trench: use of deep-sea turbidite records to reconstruct past large earthquakes. *Geol Soc Lond Spec Publ* 456:75–89. <https://doi.org/10.1144/SP456.9>
- Ikehara K, Usami K, Kanamatsu T (2023) How large peak ground acceleration by large earthquakes could generate turbidity currents along the slope of northern Japan Trench. *Prog Earth Planet Sci* 10:8. <https://doi.org/10.1186/s40645-023-00540-8>
- Johnson JE, Phillips SC, Clyde WC, Giosan L, Torres ME (2021) Isolating detrital and diagenetic signals in magnetic susceptibility records from methane-bearing marine sediments. *Geochem Geophys Geosyst* 22:e2021GC009867. <https://doi.org/10.1029/2021GC009867>
- Kanamatsu T, Usami K, McHugh CMG, Ikehara K (2017) High-resolution chronology of sediment below CCD based on Holocene paleomagnetic secular variations in the Tohoku-oki earthquake rupture zone. *Geochem Geophys Geosyst* 18:2990–3002. <https://doi.org/10.1002/2017GC006878>
- Kanamatsu T, Ikehara K, Hsiung KH (2023) Stratigraphy of deep-sea marine sediment using paleomagnetic secular variation: refined dating of turbidite relating to giant earthquake in Japan Trench. *Mar Geol* 443:106669. <https://doi.org/10.1016/j.margeo.2021.106669>
- Kawamura K, Kanamatsu T, Oishi M, Yamano M (2015) Physical and magnetic properties in piston core samples collected from the Japan Trench before the 2011 Tohoku earthquake. *JAMSTEC-R* 20:51–60. <https://doi.org/10.5918/jamstecr.20.51>
- King J, Banerjee SK, Marvin J, Özdemir Ö (1982) A comparison of different magnetic methods for determining the relative grain size of magnetite in natural materials: some results from lake sediments. *Earth Planet Sci Lett* 59:404–419. [https://doi.org/10.1016/0012-821X\(82\)90142-X](https://doi.org/10.1016/0012-821X(82)90142-X)
- Khokhlov A, Hulot G (2016) Principal component analysis of palaeomagnetic directions: converting a maximum angular deviation (MAD) into an  $\alpha_{95}$  angle. *Geophys J Int* 204:279–291. <https://doi.org/10.1093/gji/ggv451>
- Kioka A, Schwestermann T, Moernaut J, Ikehara K, Kanamatsu T, Eglinton TI, Strasser M (2019) Event stratigraphy in a Hadal oceanic trench: the Japan Trench as sedimentary archive recording recurrent giant subduction zone earthquakes and their role in organic carbon export to the deep sea. *Front Earth Sci* 7:319. <https://doi.org/10.3389/feart.2019.00319>
- Kobayashi K, Nakanishi M, Tamaki K, Ogawa Y (1998) Outer slope faulting associated with the western Kuril and Japan trenches. *Geophys J Int R Astron Soc Lond* 134:356–372
- Kodaira S, Fujiwara T, Fujie G, Nakamura Y, Kanamatsu T (2020) Large coseismic slip to the trench during the 2011 Tohoku-Oki earthquake. *Annu Rev Earth Planet Sci* 48:321–343. <https://doi.org/10.1146/annurev-earth-071719-055216>
- Korte M, Donadini F, Constable CG (2009) Geomagnetic field for 0–3 ka: 2. A new series of time-varying global models. *Geochem Geophys Geosyst* 10:Q06008. <https://doi.org/10.1029/2008GC002297>
- Lurcock PC, Wilson GS (2012) PuffinPlot: A versatile, user-friendly program for paleomagnetic analysis. *Geochem Geophys Geosyst* 13:Q06Z45. <https://doi.org/10.1029/2012GC004098>
- McHugh CM, Seeber L, Braudy N, Cormier MH, Davis MB, Diebold JB, Dieu-donne N, Douilly R, Gulick SPS, Hornbach MJ, Johnson HE, Mishkin KR, Sorlien CC, Steckler MS, Symithe SJ, Templeton J (2011) Offshore sedimentary effects of the 12 January Haiti earthquake. *Geology* 39:723–726. <https://doi.org/10.1130/G31815.1>
- McHugh CM, Kanamatsu T, Seeber L, Bopp R, Cormier M-H, Usami K (2016) Remobilization of surficial slope sediment triggered by the A.D. 2011 Mw9 Tohoku-Oki earthquake and tsunamis along the Japan Trench. *Geology* 44:391–394. <https://doi.org/10.1130/G37650.1>
- McHugh CM, Seeber L, Rasbury T, Strasser M, Kioka A, Kanamatsu T, Ikehara K, Usami K (2020) Isotopic and sedimentary signature of megathrust ruptures along the Japan subduction margin. *Mar Geol* 428:106283. <https://doi.org/10.1016/j.margeo.2020.106283>
- Mitsuzawa K, Holloway G (1998) Characteristics of deep currents along trenches in the northwest Pacific. *J Geophys Res* 103(13):13085–13092
- Moreno E, Caroir F, Fournier L, Fauquembergue K, Zaragosi S, Joussain R, Colin C, Blanc-Valleron MM, Baudin F, De Garidel-Thoron T, Valet JP, Bassinot F (2020) Magnetic fabric of Bengal fan sediments: holocene record of sedimentary processes and turbidite activity from the Ganges-Brahmaputra river system. *Mar Geol* 430:106347. <https://doi.org/10.1016/j.margeo.2020.106347>
- Morena P, Ratzov G, Cattaneo A, Klingelhoefer F, Beck C, Seibert C, Marcaillou B, Feuillet N (2022) Coexistence of adjacent siliciclastic, carbonate, and mixed sedimentary systems: an example from seafloor morphology in the northern lesser Antilles Forearc. *Front Earth Sci* 10:834029. <https://doi.org/10.3389/feart.2022.834029>
- Okuno M, Nakamura T, Sakamoto M, Yatsuzuka S, Oikawa T, Geshi N, Hoshino Y, Takahashi T (2019) Eruption age of the Haruna Futatsudake Pumice (Hr-FP), central Japan, by radiocarbon wiggle matching with special reference to a 14C dataset developed from a Japanese tree. *Quatern Int* 527:29–33. <https://doi.org/10.1016/j.quaint.2018.12.023>
- Owens WB, Warren BA (2001) Deep circulation in the northwest corner of the Pacific Ocean. *Deep Sea Res* 48:959–993
- Pares JM (2015) Sixty years of anisotropy of magnetic susceptibility in deformed sedimentary rocks. *Front Earth Sci* 3(4):1–13. <https://doi.org/10.3389/feart.2015.00004>
- Patacci M, Haughton P, Mccaffrey W (2015) Flow behavior of ponded turbidity current. *J Sediment Res* 85:885–902. <https://doi.org/10.2110/jsr.2015.59>
- Polonia A, Nelson CH, Romano S, Vaianni SC, Colizza E, Gasparotto G, Gasperini L (2017) A depositional model for seismo-turbidites in confined basins based on Ionian Sea deposits. *Marine Geol* 384:177–198. <https://doi.org/10.1016/j.margeo.2016.05.010>
- Sagnotti L, Caricchi C (2018) StratFit: an excel workbook for correlation of multiple stratigraphic trends. *Ann Geophys* 61(3):DA341. <https://doi.org/10.4401/ag-7619>
- Sawai Y (2020) Subduction zone paleoseismology along the Pacific coast of northeast Japan: progress and remaining problems. *Earth Sci Rev* 208:103261. <https://doi.org/10.1016/j.earscirev.2020.103261>
- Schwestermann T, Eglinton TI, Haghipour N, McNichol AP, Ikehara K, Strasser M (2021) Event-dominated transport, provenance, and burial of organic carbon in the Japan Trench. *Earth Planet Sci Lett* 563:116870. <https://doi.org/10.1016/j.epsl.2021.116870>
- Soda T (1989) Two 6th century eruptions of Haruna Volcano, central Japan. *Quat Res (Daiyonki-kenkyu)* 27(297):e312 in Japanese with English abstract
- Stoner JS, Channell JET, Hillaire-Marcel C (1996) The magnetic signature of rapidly deposited detrital layers from the deep Labrador Sea: relationship to North Atlantic Heinrich layers. *Paleoceanography* 11:309–325
- Strasser M, Kölling M, dos Santos Ferreira C, Fink HG, Fujiwara T, Henkel S, Ikehara K, Kanamatsu T, Kawamura K, Kodaira S, Römer M, Wefer G, RV Sonne Cruise SO219A, JAMSTEC Cruise MR12-E01 scientists (2013) A slump in the trench: Tracking the impact of the 2011 Tohoku-Oki earthquake. *Geology* 41(8):935–938. <https://doi.org/10.1130/G34477.1>

- Taira A, Scholle PA (1979) Deposition of resedimented sandstone beds in the Pico Formation, Ventura Basin, California, as interpreted from magnetic fabric measurements. *GSA Bull* 1979 90:952–962. [https://doi.org/10.1130/0016-7606\(1979\)902.0.CO;2](https://doi.org/10.1130/0016-7606(1979)902.0.CO;2)
- Tanty C, Valet JP, Carlut J, Bassinot F, Zaragosi S (2016) Acquisition of detrital magnetization in four turbidites. *Geochem Geophys Geosyst* 17:3207–3223. <https://doi.org/10.1002/2016GC006378>
- Tarling D, Hrouda F (1993) The magnetic anisotropy of rocks. Chapman and Hall, London
- Usami K, Ikehara K, Kanamatsu T, McHugh CM (2018) Supercycle in great earthquake recurrence along the Japan Trench over the last 4000 years. *Geosci Lett* 5:11. <https://doi.org/10.1186/s40562-018-0110-2>
- Usami K, Ikehara K, Kanamatsu T, Kioka A, Schwestermann T, Strasser M (2021) The link between upper-slope submarine landslides and mass transport deposits in the hadal trenches. In: Sassa K, Mikoš M, Sassa S, Bobrowsky PT, Takara K, Dang K (eds) Understanding and reducing landslide disaster risk. WLF 2020. ICL contribution to landslide disaster risk reduction. Springer, Cham. [https://doi.org/10.1007/978-3-030-60196-6\\_26](https://doi.org/10.1007/978-3-030-60196-6_26)
- Yakupoğlu N, Henry P, Uçarkuş G, Eriş KK, Demory F, Crouzet C, Çağatay MN (2022) Factors affecting thickness and frequency of turbidites triggered by earthquakes in Kumburgaz Basin, Sea of Marmara. *Mar Geol*. <https://doi.org/10.1016/j.margeo.2022.106900>
- Yoshikawa S (1976) The volcanic ash layers of the Osaka Group. *J Geol Soc Jpn* 82:497e515 in Japanese with English abstract

### Publisher's Note

Springer Nature remains neutral with regard to jurisdictional claims in published maps and institutional affiliations.

Submit your manuscript to a SpringerOpen<sup>®</sup> journal and benefit from:

- Convenient online submission
- Rigorous peer review
- Open access: articles freely available online
- High visibility within the field
- Retaining the copyright to your article

---

Submit your next manuscript at ► [springeropen.com](https://www.springeropen.com)

---